Contents list available at CBIORE journal website

International Journal of Renewable Energy Development

Journal homepage: https://ijred.cbiore.id

Research Article

Optimised PCBM electron transport layer in inverted lead-free $Cs_3Bi_2I_9$ flexible perovskite solar cells via FIRA

Adamu Ahmed Goje[a,b], Norasikin Ahmad Ludin[a*], Ubaidah Syafiq[a], Mohd Sukor Su'ait[a], Suhaila Sepeai[a], Puvaneswaran Chelvanathan[a], Matthew Davies[c]

[a] *Solar Energy Research Institute (SERI), Universiti Kebangsaan Malaysia, 43600, Bangi, Selangor Darul Ehsan, Malaysia.*

[b] *Department of Science Laboratory Technology, Federal Polytechnic Damaturu, Yobe State Nigeria.*

[c] *SPECIFIC IKC, Materials Research Centre, College of Engineering, Swansea University Bay Campus, Fabian Way Institution, Swansea SA1 8EN, United Kingdom*

Abstract. Flexible perovskite solar cells (FPSCs) offer significant versatility for portable and wearable technologies owing to their light weight, easy fabrication, low cost, and bendable properties. However, the commercialization of FPSCs faces challenges, particularly in terms of electron extraction efficiency and charge recombination, which impact device stability. Traditional high-temperature annealing methods are impractical for FPSCs due to their high energy consumption and environmental concerns. This study introduces a novel approach using flash infrared annealing (FIRA) to optimize a [6,6]-phenyl C61 butyric acid methyl ester (PCBM) electron transport layer (ETL) for lead-free cesium bismuth iodide ($Cs_3Bi_2I_9$) FPSC fabrication. The optimal FIRA conditions, 500 watts of power, PCBM concentration of 0.135 mol/L, and a 2-second annealing time were determined to enhance electron extraction, reduce charge recombination, and improve the overall device efficiency. Characterisation techniques, including UV-vis spectroscopy, photoluminescence, X-ray diffraction (XRD), and scanning electron microscopy (SEM), confirmed these optimisations. The optimised device achieved a power conversion efficiency (PCE) of 1.08%. By optimising the PCBM ETL FIRA, the PCE of lead-free $Cs_3Bi_2I_9$ FPSC was enhanced from 0.10% to 1.08%, representing a good improvement, along with a significant enhancement in electron extraction. These findings highlight the potential of optimised PCBM layers to improve the performance of FPSCs and contribute to their commercial viability.

Keywords: Electron transport layer, PCBM, Flexible perovskite solar cell, Flash Infrared Annealing

Received: 7th Sept 2024; Revised: 18th March 2025 ; Accepted: 27th April 2025; Available online: 6rd May 2025

1. Introduction

The exceptional properties of organic-inorganic lead halide perovskites as ~~the~~ active layer and perovskite solar cells (PSCs) have attracted much attention in third-generation photovoltaic systems. These include their unique features, such as cost-effectiveness, high PCE, prolonged carrier diffusion length, variable spectrum absorption range, and simple preparation. Due to their unique combination of properties, organic-inorganic lead halide perovskites hold great promise as ~~a~~ materials for practical and financially feasible solar cell technology (Wang *et al*., 2020; Zhang *et al.,* 2020; Mali *et al.,* 2018). The efficiency of perovskite photovoltaic systems has increased significantly over the last ten years, from 3.8% to an outstanding 26.1% (Goje *et al.,* 2024). PSCs have attracted considerable attention as a potential replacement for traditional silicon-based solar cells because of their affordability and remarkable power conversion efficiency. The ETL is an integral part of PSC devices, because the efficiency and stability of PSCs depend on the ETL used (Mohamad Noh *et al.,* 2018a).

However, PSC stability presents a significant challenge because degradation occurs mainly at the ETL interface (Kong *et al.,* 2021). A normal PSC electron-absorber-hole (n-i-p) typically has a structure with fluorine-doped tin oxide (FTO) as the front contact, a metal electrode, an ETL, a hole-transporting layer (HTL), and a perovskite layer. Many electron-transporting materials, including PCBM, titanium dioxide (TiO_2), zinc oxide (ZnO), stannic oxide (SnO_2), and niobium pentoxide (Nb_2O_5), have been used as ETLs because of their exceptional qualities in promoting electron transport inside the devices (Goje *et al.,* 2023; Ramli *et al.,* 2019; Bouhjar *et al.,* 2020; Taheri *et al.,* 2021; Ye *et al.,* 2020; Zhong *et al.,* 2020a). Another study investigated the role of the TiO_2 ETL in PSCs and how these functions affect the stability and performance of the device. It also examine the possibility of using inorganic materials such as ZnO, SnO_2, and barium stannate ($BaSnO_3$) as substitute ETLs in PSCs (Mohamad Noh *et al.,* 2018b). One commonly used ETL in PSCs is PCBM (Yang *et al.,* 2019a). The processing conditions used to fabricate the PCBM ETL can also significantly effect the performance and stability of FPSCs (Wang *et al.,* 2021). A vital function of the ETL is to facilitate the efficient transport of electrons generated by the absorber layer into the electrodes (Bouhjar *et al.,* 2020). Numerous efforts have been made to optimise the PCBM ETL in photovoltaic devices (Lu *et al.,* 2017; Namkoong *et al.,* 2018). PCBMs have become famous as ETL because of their high electron mobility and ease of processing

* Corresponding author
Email: sheekeen@ukm.edu.my (N.A.Ludin)

https://doi.org/10.61435/ijred.2025.60629
ISSN: 2252-4940/© 2025.The Author(s). Published by CBIORE

(Zhong *et al.,* 2020a). Optimising the PCBM ETL typically involves several critical factors, including the choice of material, the thickness of the layer (Bag *et al.,* 2020), and the processing conditions (Krebs, 2009). In recent years, several studies have explored the impact of these factors on the performance of photovoltaic devices. The materials used in these studies include indium tin oxide-coated polyethylene naphthalene (PEN/ITO) substrates, PCBM, and TiO_2. One standard method for optimising a PCBM ETL is to control the thickness of the layer. For example, in a study by Cho *et al.* (2018), the thickness of the PCBM layer varied from 40 to 120 nm, while the thickness of the TiO_2 layer was kept constant at 50 nm. Researchers found that the photovoltaic device performance improved as the thickness of the PCBM layer increased (Cho *et al*., 2018). Another study demonstrated the potential of magnetron sputtering in fabricating efficient perovskite solar cells while investigating its impact on the organic transport layer, achieving a notable PCE of 18.35% (Eze *et al.,* 2021).

The choice of material and fabrication procedure is a critical factor in optimizing the PCBM ETL. PCBM has shown promise as an ETL because of its ability to enhance the stability and efficiency of PSCs. Various factors must be considered to optimize the PCBM ETL in FPSCs, such as the thickness and surface roughness of the layer, coverage, and grain. The characteristics and performance of PCBM layers have been the subject of numerous investigations.

To create layers that are consistent and under strict control, researchers investigated into a variety of fabrication methods, including spin-coating (Gao & Meng, 2020), roll-to-roll (Tzounis *et al.,* 2017), doctor-blading (Zhong *et al.,* 2020a), and vacuum deposition (Li *et al.,* 2022). With the help of these procedures, layer morphology and thickness can be precisely controlled (Bag *et al.,* 2020), which impacts the effectiveness of charge extraction and transport. The PCBM concentrations significantly affect the efficiency of the electron transport layer. The performance of the electron transport layer (ETL) substantially influences the entire device's efficiency, stability, and flexibility. Therefore, enhancing the PCBM concentration increases the electron transport and charge extraction efficiency, improving device performance overall (Yang *et al*., 2019a).

Furthermore, to improve the charge transfer and reduce recombination losses, the compatibility and interfacial characteristics between the low-temperature process PCBM layers were investigated with an efficiency of 16.11% (Yang *et al*., 2021). Research has also been conducted to determine how the PCBM layer affects the flexibility and stability of devices. The electron transport layer must be mechanically robust and resilient to bending or stretching for use in flexible perovskite solar cells (Fan *et al*., 2016). Coa *et al.* concentrated on creating methods to improve the TiO_2 layer's adherence to the flexible substrate and optimizing the composition and thickness to withstand mechanical stress while retaining effective charge transmission (Cao *et al.,* 2015).

FIRA is a rapid and antisolvent (AS) free technique capable of generating highly crystalline perovskite films in under 2 seconds, yielding efficiencies exceeding 20%. Its adaptability for continuous processing and avoidance of prolonged annealing steps are promising alternative (Ling *et al*., 2021). It has emerged as a swift technique for producing perovskite solar cells, achieving efficiencies exceeding 18% with a synthesis time of merely 1.2 seconds. In contrast to the conventional AS method at the lab scale, FIRA displays substantial advantages, boasting an environmental impact of only 8% and reducing fabrication costs by 2% for the perovskite active layer. This highlights its potential as a cost-effective, eco-friendly approach that is well-suited for industrial scaling (Sánchez *et al.,* 2019).

The paper introduces the FIRA method for rapid, efficient production of stable, high-efficiency FPSCs. This technique allows the annealing of the PCBM layer in seconds, ensuring continuous and synchronised manufacturing while optimising new perovskite compositions based on formamidinium lead iodide and a passivation treatment to enhance the film quality. The study marks a significant advancement in using FIRA for industrial-scale production of PSCs, offering the potential for large-scale commercialisation (Sánchez, Jerónimo-Rendon, *et al*., 2020a).

Compared to conventional hot-plate annealing, the inherent mechanism of PCBM ETL behavior when annealed with FIRA has various benefits; the chief among them is an improvement in the efficiency of organic photovoltaics (Sánchez, Jerónimo-Rendon *et al.,* 2020a). Morphological and electrical characteristics of PCBM ETLs are significantly affected by FIRA, which is distinguished by rapid thermal processing using infrared radiation, resulting in improved device performance (Ling *et al*., 2021). Its capacity to produce even heat throughout the PCBM layer is one of its main advantages (Wang *et al.,* 2020). The FIRA process provides uniform thermal exposure, promoting consistent molecular ordering and crystallinity within the PCBM layer, which enhances the charge transport and overall device efficiency. Its rapid heat cycles prevent the degradation of temperature-sensitive organic components, preserving the quality of active layer materials and improving long-term device stability (Gao *et al.,* 2018).

Additionally, FIRA improves interfacial adhesion between layers, reduces resistance, and enhances charge transfer, leading to higher power conversion efficiencies and making it suitable for large-scale production. The FIRA process is known for its ability to selectively heat materials via radiation (Ling *et al.,* 2021). This leads to controlled crystallisation without causing thermal damage to the underlying flexible substrate, which is a critical requirement for FPSCs (Sánchez, Hua, *et al.,* 2020). The crystallisation of PCBM, however, needs to be meticulously regulated, as uncontrolled crystallisation can lead to the formation of large PCBM crystals. These large crystals disrupt the smoothness of the ETL, creating energy barriers and recombination sites, which in turn reduce the overall efficiency of the solar cell. FIRA annealing plays a pivotal role in this regulation. By applying far-infrared radiation, it selectively heated the PCBM layer, promoting the formation of a uniform crystalline structure without affecting the flexible substrate. This results in a smoother and more homogenous ETL, which is crucial for efficient electron transport and minimal energy loss. Moreover, controlled crystallisation achieved through FIRA can significantly enhance the open-circuit voltage (V_{OC}) of PSCs. A well-crystallised PCBM layer reduces the likelihood of trap states at the interface, which is often the cause of nonradiative recombination losses. This improved Voc is a direct consequence of the high-quality interface between the perovskite layer and the PCBM ETL.

Presently, research in FPSCs has explored several types of materials besides PCBM, including ZnO (Bouhjar *et al.,* 2020), SnO_2 (Bi *et al.,* 2021), and TiO_2 (Shahiduzzaman *et al.,* 2021), which have drawn attention to their better electron mobility and stability when exposed to UV radiation. An additional example is ZnO, which has ideal electron mobility and transparency but is chemically unstable in acidic environments, which might hasten the degradation of perovskite layers (Malison *et al.,* 2019). However, because of its wide bandgap, low processing

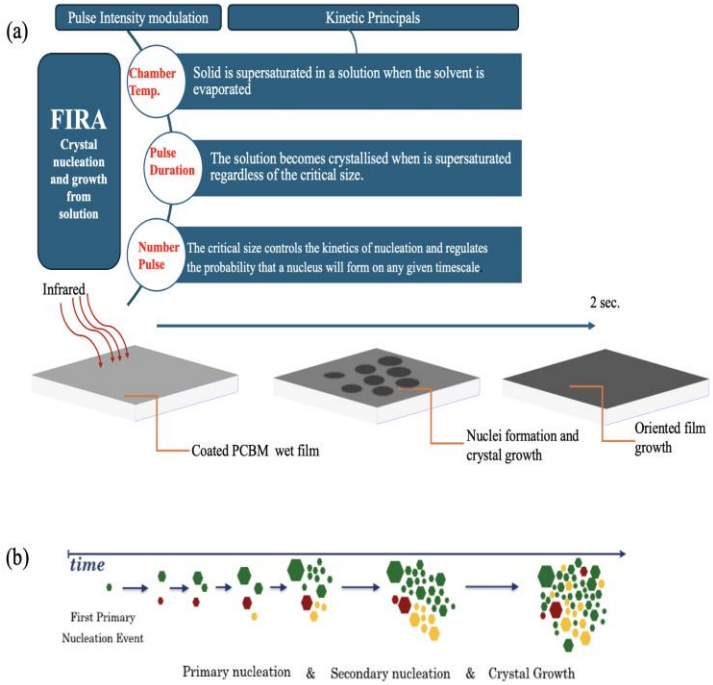

Fig. 1. a) FIRA Process for Crystal Nucleation and Growth in PCBM Films b) Diagram showing the crystallisation of system nucleation and growth.

temperature, and excellent optical transparency, SnO_2 has become a viable substitute ETL material that is also good for FPSCs (Noh *et al.,* 2020)[38]. Researchers are also investigating materials like niobium pentoxide (Nb_2O_5) and barium stannate ($BaSnO_3$) because they can enhance the stability and performance of devices (Wenqi Zhang, 2022). Rapid thermal processing (RTP) and rapid annealing methods (Ouyang *et al.*, 2020) and microwave-assisted annealing (Wang *et al.,* 2022) are also being investigated for their ability to improve the overall quality of the perovskite films and speed the fabrication process.

Figure 1a illustrates the FIRA process for controlling the crystallisation of PCBM in the ETL on a flexible substrate, which is critical for the fabrication of efficient FPSC. The process begins with a coated PCBM wet film that is selectively heated by infrared radiation. This induces nucleation and controlled crystal growth, preventing large crystal formation that could disrupt the ETL smoothness and decrease the solar cell's efficiency. Over 2 s, the process led to oriented film growth, which enhanced the quality of the ETL by maintaining uniformity and minimising energy loss during electron transport. The critical parameters of the FIRA process—chamber temperature, pulse duration, and pulse number were carefully regulated to ensure optimal crystallisation.

Figure 1b shows the crystal development and secondary nucleation deterministically within the framework of population balance equations, treating each new primary nucleus as developing stochastically (Maggioni & Mazzotti, 2019). Particles diffuse to the surface of the pre-existing nucleus and integrate into the crystal lattice structure during the development stage, which follows nucleation. The crystal's size distribution and structure were determined during the early phases of solution crystallisation (Zhang *et al.,* 2021). The primary supposition for crystal formation is that stable nuclei exist before growth and molecules join stable clusters under the influence of a phase's decreasing Gibbs free energy, albeit kinetically constrained. The Johnson–Mehl–Avrami equation can be used to study the crystal shape. For a fresh K-phase, the volume transformation Vx as a function of time is given by Eq 1.

$$x(t) = 1 - \exp[-(\beta)^N] \quad (1)$$

Particle shape in the β-phase affects the parameter N N. Spherical particles have N = 3, disk-shaped particles have N = 2, and rod-shaped particles have N = 1. The transformation rates are slow at the beginning and end, but quickly rise in the middle stage. The early slow rate is evident because it takes enough nuclei to develop in the subsequent phase. The transition increases as the nuclei expand into new particles during the intermediate stage. While some nuclei move into the development phase, others remain to form initially. Nuclei that have not yet transformed slows the creation of new particles when the transformation approaches completion (Jackson, 2004). PCBM was deposited onto the absorber layer using the FIRA annealing technique. This method involves the controlled application of a PCBM solution onto the substrate, that is annealing the substrate at different FIRA powers (420 W to 556 W), as shown in Figure 1. A Lower power allows for slower and gentler solution heat penetration, potentially forming thicker and more irregular films.

Conversely, a higher power encourages the rapid heating of the solution, resulting in thinner and more uniform films. Each power represents a specific set of conditions affecting the solvent evaporation rate, distribution of PCBM molecules, and ~~the~~ overall film morphology, which will be described later in various Characterisations. The optimal power depends on balancing these factors to create a film with desired properties, such as uniformity and crystallinity. Notably, the power choice affects the performance of the resulting PCBM.

The limitation of FPSC fabrication is their reliance on traditional annealing processes. Hot plate fabrication and other traditional perovskite layer fabrication techniques sometimes require temperatures of approximately 150 °C and lengthy processing times, which may affect the quality of flexible substrates like PEN and PET (Aftab *et al.,* 2024). The mechanical flexibility and long-term durability of FPSCs, which are both

crucial for wearable and portable applications, are limited by the substrate deformation caused by these high temperatures. Additionally, extended exposure to high temperatures may accelerate device degradation by causing unexpected interface reactions (Corzo *et al.,* 2020).

Numerous challenges exist when hot plates are used in traditional annealing procedures to fabricate FPSC. Hot plate heating is a slow process that requires a long time to guarantee even heat distribution throughout the layers, which may impact the scalability and reproducibility of the fabrication process (Ling *et al.,* 2021). Furthermore, the slow heating rate incresease the possibility of uneven crystallisation in the PCBM ETL layer, which could result in defects that lower the stability and efficiency of the device (Namkoong *et al.,* 2018). In addition, hot plate heating might unintentionally affect other layers in the solar cell system, especially the organic transport layers that are sensitive to temperature changes, because it is not precise enough to target particular layers (Wang *et al*., 2013; Isah *et al.,* 2024). The FIRA process was recently introduced as a more accurate, efficient, and substrate-friendly alternative to hot-plate annealing. FIRA can anneal materials quickly in a few seconds, minimising the thermal stress on flexible substrates using less energy. (Sánchez, Jerónimo-Rendon, *et al*., 2020b). This technique enables greater control over layer morphology, producing highly crystalline films with fewer defects, which enhances the stability and performance of the device (Sanchez, 2020). Furthermore, FIRA's quick processing time and reduced heat exposure benefit flexible substrates such as PEN/ITO, which might deteriorate when exposed to conventional high-temperature annealing techniques that take longer (Ling *et al.,* 2021). As a result, FIRA offers a potential way to overcome the challenges of hot plate-based annealing, which makes it a good choice for fabricating high-performance FPSCs on an industrial scale (Sánchez, Jerónimo-Rendon, *et al.,* 2020b).

This work reveals the significance of enhancing the PCBM ETL layer for the optimum efficiency of an inverted FPSC. The systematic inquiry was based on the results of previous research. This is the first time that PCBM was optimized on a PEN/ITO/PEDOT: PSS/$Cs_3Bi_2I_9$ layer flexible substrate using FIRA; various characterization techniques were used to investigate the PCBM ETL. Light absorption, transmission, and emission properties were examined using optical characterization techniques, such as UV-Vis and PL spectroscopy. The ETL morphology, crystallinity, and interfacial characteristics were extensively studied using the XRD. At the same time, the surface's thickness and roughness were assessed by the AFM, and the final result shows the power to be used in the fabrication of FPSC with PCBM ETL using FIRA for the first time..

2. Experimental

2.1 Materials and Solvents

PEN/ITO with 80% transparency, dimensions of 29.7 cm × 21 cm × 125 µm thickness, and sheet resistance below 15 Ω/sq was procured from Sigma Aldrich, USA (917826-1EA). Materials including poly (3,4-ethylene dioxythiophene) poly (styrene sulfonate) (PEDOT, AI4083, Sigma-Aldrich), Cesium iodide (CsI) 99.9%, Bismuth iodide (BiI_3) 99%, lithium bis (trifluoromethane sulfonyl) imide (Li-TFSI, 99%), text-butyl pyridine (tBp, 96%), and 2,2′,7,7′-tetrakis(N, N-di-p-methoxyphenylamine)-9,9′-spirobifluorene were also purchased from Sigma–Aldrich. Absolute ethanol, anhydrous N, N-dimethylformamide (DMF, 99.8%), and chlorobenzene (99%) were purchased from R&M Chemicals. Polyethyleneimine (80% ethoxylated solution, 35-40 wt. % in H2O) and 4-tertbutylpyridine (TBP) were obtained from Sigma-Aldrich. All chemicals were used as received without further treatment or purification.

2.2 Device Fabrication

FPSCSs were fabricated utilising device configurations involving PEN/ITO/TiO_2/PCBM/ $MAPbI_3$/Spiro-OMeTAD/Ag. The PEN/ITO substrate underwent etching through zinc powder and HCl, followed by cleaning using ethanol, acetone, and isopropanol in an ultrasonic bath at 50°C temperature for 15 minutes each. The substrate was then washed with deionised water, dried using nitrogen flow, and treated with 5 minutes of ozone plasma to eliminate organic residues and wettability. The fabrication of the inverted FPSC structure comprising PEN/ITO/PEDOT: PSS/$Cs_3Bi_2I_9$/PCBM/Ag included the application of PEDOT: PSS HTL onto the PEN/ITO surface via spin-coating at 4500 rpm for 30 seconds, followed by annealing at 150 °C for 30 minutes in ambient air (Yang *et al.,* 2019b). A precursor solution for $Cs_3Bi_2I_9$ was developed by dissolving a mixture of BiI_3 (1.65

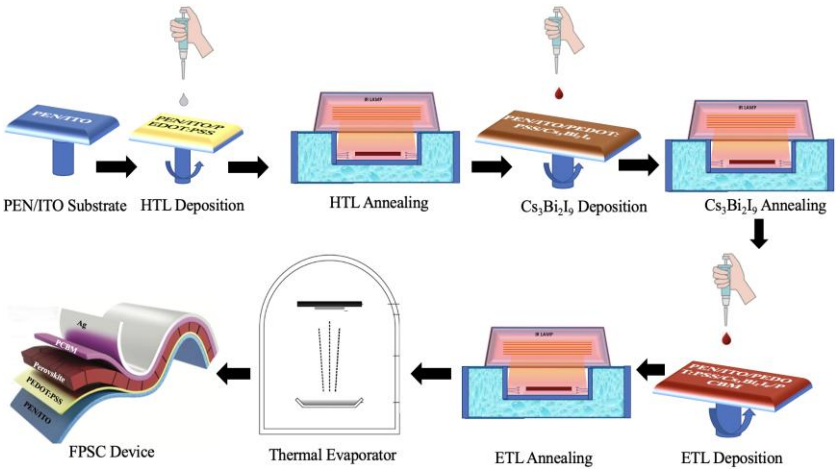

Fig 2. (a) PCBM ETL (b) PCBM annealing using FIRA (b). Perovskite Deposition and annealing (c). HTL Deposition (d). Ag Deposition via thermal evaporation

Fig 3. FIRA system used in the annealing of the PCBM ETL (a) control unit (b) annealing chamber (c) system specification (d) FPSC being annealed in the chamber

Table 1
Power variation for annealing PCBM ETL

Power (W)	Corresponding Temperature (° C)	Measurement Uncertainty (± W)	Measurement Uncertainty (°C)	Thermal Coefficient (W/°C)
420	90	±5	±1	6.00
444	95	±5	±1	5.55
472	100	±5	±1	5.24
500	105	±5	±1	5.00
528	110	±5	±1	4.80
556	115	±5	±1	4.63

M) and CsI (2.475 M) in DMF and stirring for over 24 hours at 70 °C. A brief annealing step of 2 seconds was executed 10 times in full power mode using the control. Concerning the ETL solution, 30 mg of PCBM was combined with 1 mL of chlorobenzene to achieve a concentration of 0.135 mol/L (Yang *et al.,* 2019b), with the power range set from (444 W to 556 W). This solution was applied onto the prepared PEN/ITO/PEDOT: PSS/$Cs_3Bi_2I_9$ through the spin coating at speeds of 3000 rpm, each for 30 seconds, and annealed with FIRA for 2 sec (x10) at a power of 500 W (Ling *et al.*, 2021). The colour transition of the surface from yellow to black was observed. Following a cooling period of 10 seconds in the oven, the samples were removed. Finally, the device was completed by depositing a silver (Ag) top electrode through thermal evaporation (Jiang *et al.,* 2018).

2.3 FIRA Methodology

The calibration of the Adphos FIRA NIR 120 M3 (Serial Number 1168) using the Fluke Ti32 Thermal Imager is crucial for ensuring accurate temperature control during the annealing process of the PCBM ETL in inverted FPSCs. Calibration involves aligning temperature readings from the thermal imager with specific power outputs, such as 444 W correlating with 90°C and 556 W with 115°C. An analysis of the imager's readings against known power inputs establishes a direct relationship between displayed temperature and supplied power. This process guarantees precise temperature monitoring, enhancing the reliability and consistency of the annealing process key for optimal control and performance of the NIR 120 M3 system.

The FIRA system has two key control parameters: power output and exposure time; both can be fine-tuned for optimised annealing, as depicted in Figure 3a. The power output is adjustable between 0-100%, while the timer allows precise regulation of the annealing duration in seconds. Temperature is directly monitored on the FIRA display, enabling real-time adjustments based on this, corresponding with the thermal imager. The distance between the infrared light source and the sample can also be controlled. This study maintained a 4 cm gap to ensure uniform heating, as illustrated in Figure 3b. Specifications of the system, including its 5.8 kW power rating, are presented in Figure 3c, while Figure 3d provides a real-time view of the annealing process for the FPSC device.

Power output was varied to determine the optimal conditions for PCBM ETL annealing in the FPSC inverted structure. Table 1 provides the relationship between power settings and corresponding temperatures, showing that as power increases from 420 W to 556 W, the temperature rises from 90 °C to 115 °C. Each power setting has an associated uncertainty of ±5 W, reflecting power supply variability. The thermal coefficient represents the rate of power change concerning temperature. The thermal coefficient decreases with rising temperature, from 6.00 W/°C at 70°C to 4.63 W/°C at 120°C, indicating that less power is required to raise the temperature further as higher levels are reached.

Optimizing control parameters, such as annealing duration and energy output, is critical to achieving uniform crystallisation in the PCBM ETL layer. Shorter annealing times (typically under 2 seconds, in 10 pulses) were optimal for maintaining material integrity while achieving the desired crystallisation. Moreover, adjusting the power output to match specific temperature targets ensures that the annealing process is energy-efficient and conducive to large-scale production.

2.4 Characterisation

The surface morphology of the sample images was observed through scanning electron microscopy (SEM; ZEISS, Merlin Compact) and Nano-surf Easyscan2 atomic force microscopy (AFM). XRD spectra were acquired using a Bruker D8 advance model at a 2θ angle. Optical absorption spectra were recorded employing a Lambda 35 Perkin Elmer UV-visible (UV-Vis) spectrophotometer. Solar simulated AM 1.5G sunlight, calibrated to provide 100 mW/cm^2 using a standard Si photovoltaic cell (Daystar Meter), was utilised. J–V curves were measured using a Keithley 2400 source meter at a scan rate of 0.1 V/s. Steady-state PL spectra were collected with a fluorescence spectrometer (FLS920, Edinburgh Instruments) using an excitation wavelength of 515 nm. All experiments were conducted under ambient air conditions without humidity control.

3. Results and Discussion

The UV-Vis spectroscopy characterising of the PCBM films annealed at different power (420 W to 556 W) were explored during FIRA annealing, with 500 W yielding the second highest transmittance, as shown in Figure 4a. This suggests good power enhances the film's light-transmitting properties due to suitable thickness and uniformity. A fabrication procedure involving PCBM utilises UV-Vis spectroscopy to analyse the thickness of thin-film devices in perovskite heterojunction solar cells. The analysis shows a transmittance of around 80%, with thicknesses ranging from 90 nm to 230 nm (Shah *et al.,* 2017). Our findings hold potential for enhancing devices like optoelectronics and photovoltaics that use such films, underlining the intricate relationship between deposition parameters and optical performance and indicating better light transmittance to the absorber layer. The obtained band gap was 1.9 eV (Figure 4b), higher than the perovskite layer, facilitating efficient electron transfer. The band gap of PCBM is usually around 2 ± 0.2 eV (Shah *et al.*, 2017). The charge carrier lifetime of PCBM annealed at 500 W was deducted in the formula in Eq 2.

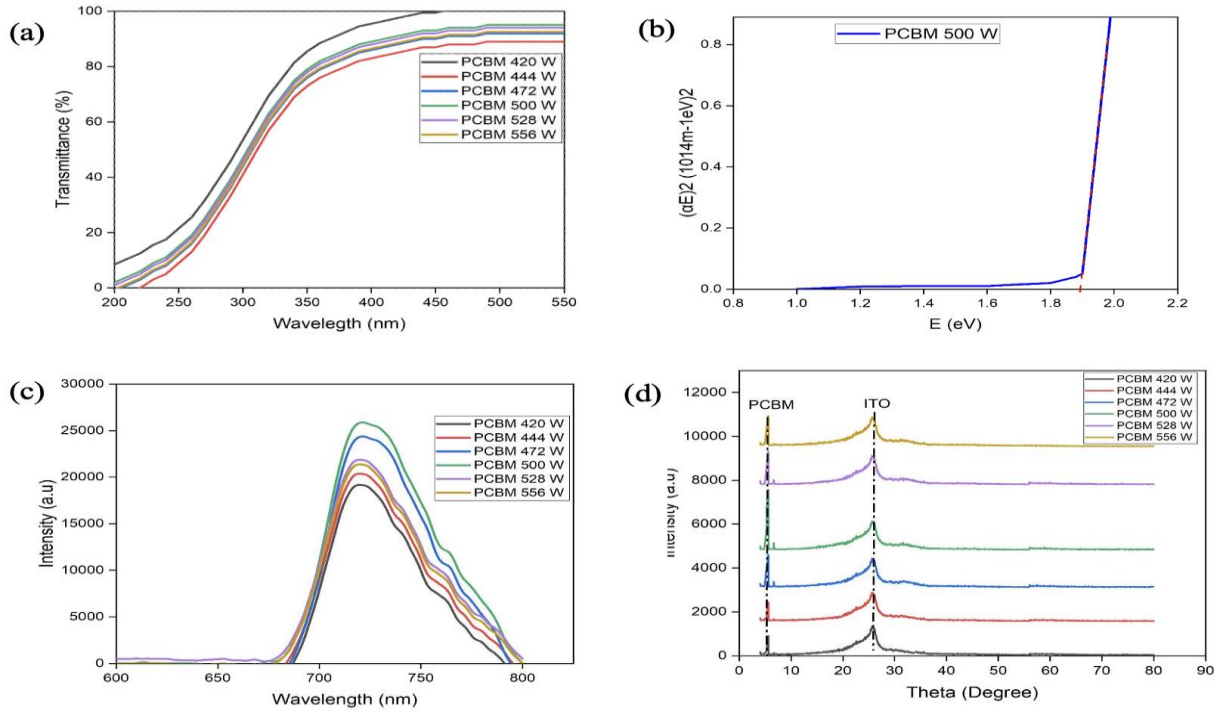

Fig 4. (a) UV Transmittance Spectrum of PCBM, (b) the band gap determination, (c) PL spectra of the PCBM ETL annealed at various power, (d) XRD patterns of PCBM films annealed at various power.

Table 2
The carrier lifetime values of the samples.

FIRA Power (Watts)	B_1	T_1	B_2	T_2	B_3	T_3	Avg. Lifetime
420	0.008	0.6447	0.112	6.2285	-0.101	6.2716	4.991
444	0.006	0.6926	-0.622	6.1858	0.622	6.1862	1.3524
472	0.011	0.6032	-0.221	3.9539	0.222	3.9549	1.9787
500	0.005	0.2218	0.009	0.6925	0	3.2371	0.6214
528	0.013	0.2234	0.0214	0.5621	0.001	3.1251	0.9512
556	0.009	0.6547	0.102	6.9585	-0.101	6.9716	2.9362

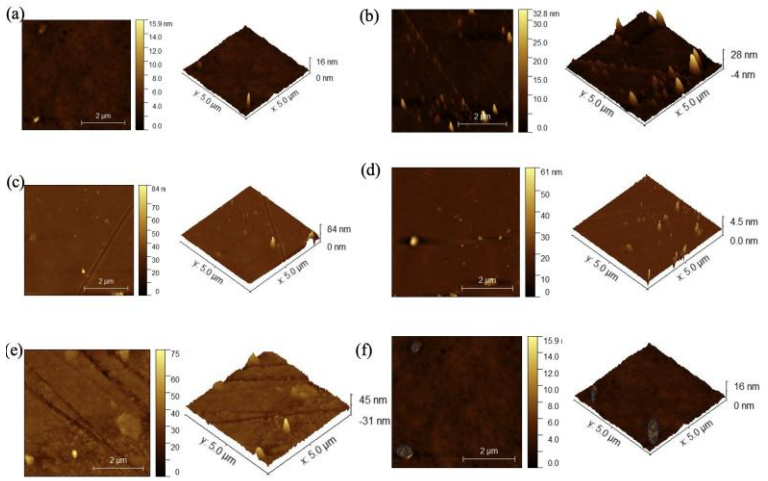

Fig 5. a–f AFM images of FIRA power at 420 W (RMS 2.50 nm), 444 W (RMS 0.50 nm), 472 W(2.14 nm), 500 W (RMS 2.04 nm), 528 W(RMS 2.30 nm), and 556 W(RMS 4.06 nm) each for 2 sec

$$\boldsymbol{\tau_{av}} = \frac{\boldsymbol{T_1B_1+T_2B_2+T_3\,B_3}}{\boldsymbol{B_1+B_2+B_3}} \quad (2)$$

where τ = B's are constant for the recombination lifetime, whereas T's are temperatures. The charge carrier lifetime is typically a measure of how long charges, in this case, electrons, persist in a semiconductor material before recombination occurs.

The photo-luminance (PL) characterisation of PCBM films at different power levels during film annealing influenced the emission properties as shown in Fig 4c. Among the investigated range of FIRA power, 500 W emerged as the most effective in producing enhanced Photo-luminance with the lower intensity and charge carrier lifetime at 0.6214 sec (Table 2). It means fast electron extraction, reduced recombination, and increased stability. This outcome is ascribed to the optimised film morphology and thickness achieved at this power, which improved the material's ability to generate and emit light efficiently. The comparison of FPSCs using PCBM layers demonstrates that PCBM diffusion into perovskite grain boundaries significantly reduces hysteresis in the J-V curve. Real-time visualisation using PL imaging microscopy shows a reduction in ionic mobility and an increased activation energy in the presence of PCBM, providing insights into the mechanism for hysteresis suppression in FPSCs; they used PCBM, a 10 mg mL^{-1} solution in chlorobenzene that was annealed at 100 °C for in the fabrication of the device (Zhong *et al.,* 2020b). These findings contribute to a deeper understanding of the relationship between film annealing and the optical properties of PCBM-based systems, with implications for better FPSC. The XRD analysis investigated the crystal structure of a PCBM film annealed using FIRA. The film results revealed that the degree of crystallinity in the PCBM film changed with different supplied power. The highest crystal value recorded was 61.7%, and the highest peak of the display was distinct (100) at 5.30°. This occurred when the film was annealed at 500 W, as shown in Figure 4d. All differences in grams in Fig. 3d are displayed at 5.30° with a distinct peak of (100) originating from the structure of PCBM, and the phase identification confirmed the presence of PCBM. This peak represents an a-axis orientation, in which the side chains align parallel to the substrate and the primary polymer chain aligns perpendicular (Erb *et al.,* 2005).

The corresponding mean size of PCBM crystallites was then estimated based on the full width at half maximum intensity of the diffraction peak, according to Scherrer's equation, L = $0.9\lambda / B_{2\theta}\cos(\theta)$, which denotes the wavelength of the X-ray and represents the diffraction angle, and $B_{2\theta}$ represents the broadening at half the maximum intensity (Karagiannidis *et al.,* 2011).

The crystal size provides a well-defined pathway and enables efficient charge extraction from the absorber layer. Molecules exhibited the highest tendency to form a well-organized and crystalline structure within the film. Hence, film treatment and molecular mobility favor the formation of a highly ordered crystal lattice. The highest level of crystallinity observed at 500 W indicates the optimal conditions for achieving a well-structured and organized PCBM film. This is good because it enables efficient electron extraction without energy losses due to backflow.

AFM was employed to investigate the influence of different FIRA power (ranging from 420 W to 556 W) on the morphology of the PCBM ETL in FPSC. The images revealed that the PCBM ETL exhibited irregularities and incomplete coverage at lower power, while higher power resulted in improved surface smoothness. The optimal results, characterised by minimal surface roughness, well-defined grain size, and uniform distribution, were consistently observed at 500 W. This power yielded a balanced compromise between layer thickness and uniformity, crucial for efficient charge transport. Furthermore, the AFM analysis highlighted a reduction in surface defects at 500 W, indicative of improved electrical properties. These findings underscore the significance of careful thermal treatment optimization, emphasizing 500 W as an ideal condition for fabricating high-performance FPSC with PCBM ETL using FIRA treatment. The study provides valuable insights for enhancing the reliability and efficiency of FPSC devices through controlled treatment parameters. The topographic viewpoint of various powers is shown in Fig 5. It can be seen that 472 W and 500 W have a much rougher surface (Mean roughness (Sa): 2.04 nm and 2.14 nm) compared to 444 W, 528 W, and 556 W (Mean roughness (Sa): 0.50 nm, 2.30 nm, and 4.06 nm).

The root means square (RMS) of the FIRA power of 472 W (2.14 nm) and 500 W (RMS 2.04 nm) is lower compared to 528 W (3.6 nm**)** to 556 W (4.06 nm) is much higher, by using the line scan analysis as displayed in Fig. 5. The advantage of the large surface particles in the thin film surface suggested that more light might be transmitted to the absorber layer. AFM force-distance graphs revealed a consistent change in stiffness

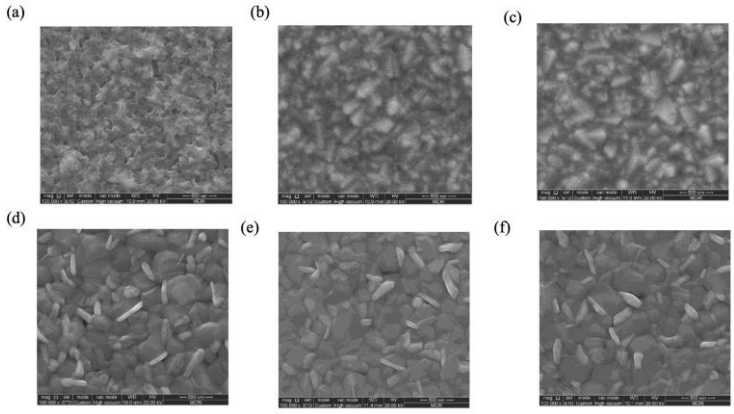

Fig 6. The surface morphology photographs of $Cs_3Bi_2I_9$ on (a) PCBM at 420 W, (b) PCBM at 444 W, c) PCBM at 472 W, (d) PCBM at 500 W, (e) PCBM at 528 W, (f) PCBM at 556 W

Table 3
The published photovoltaic performances of lead-free $Cs_3Bi_2I_9$ PSCs fabricated to date.

$Cs_3Bi_2I_9$ /PCBM ETL Device structure	**Voc (V)**	**Jsc(mA/cm^2)**	**FF**	**PCE**	**Ref.**
ITO/PEDOT:PSS/$Cs_3Bi_2I_9$/PCBM/Ag	0.69	2.31	1.08	47	**This work**
ITO/PEDOT:PSS/ $Cs_3Bi_2I_9$/PCBM/Ag	0.55	1.50	80	1.20	(Bai *et al.,* 2018)
FTO/C-TiO_2/$Cs_3Bi_2I_9$/PCBM/Ag	0.90	6.00	65	3.50	(Waykar *et al.,* 2020)
ITO/NiO/$Cs_3Bi_2I_9$/PCBM/Ag	0.65	2.80	50	0.90	(Vijaya *et al.,* 2023)
ITO/NiO/$Cs_3Bi_2I_9$/PCBM/Ag	0.62	2.40	47	0.70	(Yu *et al.,* 2019)
ITO/NiO_x/$Cs_3Bi_2I_9$/PCBM/Ag	0.64	3.15	57	1.15	(Hamukwaya *et al.,* 2022)
FTO/C-TiO2/M-TiO_2/$Cs_3Bi_2I_9$/PCBM/Carbon	1.05	4.00	75	2.90	(Khadka *et al.,* 2019)

surrounding the PCBM crystals due to decreased PCBM concentration near the crystals. Moreover, variations exist on the surface concerning the annealing temperature (Karagiannidis *et al.,* 2011). The spin-coating approach reveals a thinner layer in both samples. The layer annealed at 472 W and 500 W is considerably thinner than at 444 W, measuring 140 nm compared to 80 and 90 nm, respectively. Typically, the PCBM ETL in PSC is between 20 and 100 nm thick. According to specific device requirements and deposition methods, this variant offers the best charge transfer and efficiency (Miller *et al.,* 2008).

SEM images were obtained to investigate the effects of changing FIRA power on PCBM film morphology. In that order, the power levels examined were 420 W to 500 W, corresponding to Fig. 6(a)–6(f). On the PCBM film annealed at 528 W, pinholes were found. Nevertheless, no pinholes were seen on PCBM thin films annealed at 472 W and 500 W. To effectively characterize the PCBM ETL, a high-resolution SEM image must have accurate surface features and few defects. It should preserve consistent repeatability while showcasing the layer's topography, surface morphology, and structural imperfections. A perfect SEM result facilitates in-depth examination, which helps to comprehend the composition, homogeneity, and suitability of the PCBM ETL for use in electronic device applications. A few pinholes formed in the compact and full-coverage perovskite film suggested increased leakage current and recombination losses in the device. The film was made of small, packed grains utilizing various power annealing temperature techniques.

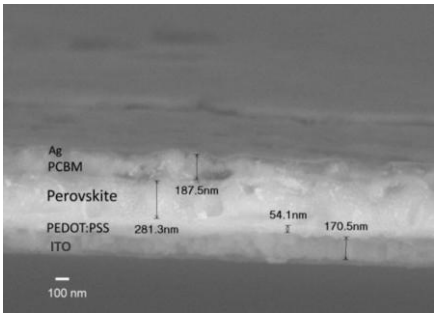

Fig. 7. Cross-Sectional SEM Image of a Layered $Cs_3Bi_2I_9$ FPSC device

In contrast, the 500 W sample's grain boundaries were far more accurate. The 444 W and 472 W film surfaces exhibit pinholes and irregular grains, indicating a weakly crystallized perovskite structure. In addition, the surface of the 500 W film was smooth and dense. Fig. 7 illustrates the thickness and function of each layer in a perovskite solar cell's layered structure. The top electrode for electron collection is the Ag layer, which has a thickness of 170.5 nm. The layer of 54.1 nm PCBM acts as the ETL underneath it, and the layer of 281.3 nm $Cs_3Bi_2I_9$ perovskite absorber. The hole transport layer facilitates hole transfer to the ITO layer below, the 187.5 nm PEDOT: PSS layer. The ITO layer is the transparent conductive electrode that facilitates light ingress and hole collection.

Table 3 summarises the photovoltaic performance of various device topologies using PCBM ETL on $Cs_3Bi_2I_9$ as the active layer. With a PCE of 3.50% and a maximum Voc of 0.90 V, the device structure FTO/C-TiO_2/ $Cs_3Bi_2I_9$/PCBM/Ag has demonstrated exemplary performance. PCE, FF, Jsc, and Voc are significant measures to consider. In contrast, the ITO/NiO/$Cs_3Bi_2I_9$/PCBM/Ag structure performed worse, with a Voc of 0.62 V and a PCE of 0.70%. These results show how

Table 4
The photovoltaic performance of the PCBM annealed with different FIRA power on $Cs_3Bi_2I_9$ FPSC.

FIRA Power (Watts)	V_{oc} (V)	J_{sc} (mA/cm^2)	PCE (%)	FF (%)
PCBM 444	0.16	0.69	0.07	44
PCBM 444	0.28	1.18	0.20	42
PCBM 472	0.46	1.29	0.42	50
PCBM 500	0.69	2.31	1.08	47
PCBM 528	0.58	1.81	0.61	41
PCBM 556	0.48	1.34	0.26	32

different PCBM-based ETLs affect the solar cell device and offer potential research avenues.

Based on different power on the PCBM ETL deposited on the absorber layer and the structure of perovskite films, the influence of the amount of technique on the photovoltaic properties of ETL film was investigated of the PEN/ITO/PEDOT: PSS/$Cs_3Bi_2I_9$/PCBM/Ag structure. The five devices were fabricated under the same conditions. The photovoltaic performances of the FPSCs were analysed under the illumination of AM 1.5G and 100 mW/cm^2. The photovoltaic performance characterization curve is shown in Fig 8 and the results are shown in Table 4. The PCE of the cells fabricated with FIRA power at 500 W was high. Table 4 shows the highest PCE of 1.08% with a J_{SC} of 2.31 mA /cm^2, a V_{OC} of 0.69 V, and an FF of 47%. This is about the smooth, compact, and large crystal at 500 W. The high V_{OC} compared to others is mainly due to the less pinhole, boundary-defect-less, and less charge recombination. Low fill factor in FPSC may arise from trap states and interface deficiencies, hindering efficient charge transport. Also, poor electrode contact and structural defects within the FPSC layer further diminish FF, impeding current flow. Optimizing those factors will improve interface quality and reduce trap states, enhancing FF and overall efficiency (Hao *et al.,* 2020). FPSCs fabricated using FIRA performance show significant advantages over traditional methods in efficiency, cost-effectiveness, environmental impact, and scalability (Sánchez et al., 2019). FIRA reduces processing time from several hours to seconds, leading to higher PCEs, with the highest PCE recorded at 1.08% at 500 W. This rapid thermal processing technique lowers energy consumption, cutting operational costs and making large-scale production more feasible. FIRA's energy-efficient process also reduces the environmental footprint, offering a more sustainable alternative to conventional methods.

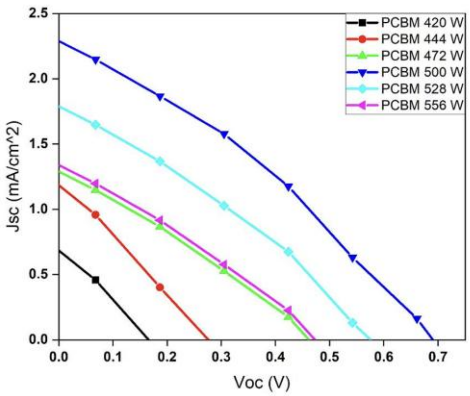

Fig 8. Photocurrent density-voltage curves of lead-free FPSCs employing different power outputs on PCBM ETL

Traditional fabrication techniques like hot plate annealing are time-consuming, energy-intensive, and not easily scalable for industrial applications. In contrast, FIRA's uniform heating across substrates supports continuous processing methods like roll-to-roll manufacturing, which is essential for the mass production of FPSCs. Furthermore, the optimised FPSCs produced with FIRA show improved charge transport and reduced recombination losses, resulting in better device performance, particularly regarding FF and V_{oc}. This demonstrates the superior potential of FIRA for scaling up flexible perovskite solar cell production while also offering a more eco-friendly and efficient alternative to traditional methods.

4. Conclusion

PCBM is a common ETL used in perovskite solar cells. PCBM is an effective electron acceptor with good electron transport properties and low processing temperature. The ETL plays a critical role in the performance of the FPSC, as it facilitates the transport of electrons from the active layer (perovskite) to the electrode. Specifically, optimized PCBM using the FIRA annealing method enhances the electron extraction efficiency, reduces charge recombination losses, and improves the device's overall stability. This article selected the PCBM ETL on – $Cs_3Bi_2I_9$ for use on an inverted heterojunction structure suitable for the low-energy and low-temperature solution method to prepare the FPSC. To solve the problems in fabricating PSCs on a rigid substrate, Low electron extraction efficiency at the ETL and High charge recombination at the PCBM ETL are required. All These problems contribute to rapid degradation and low efficiency. For the device optimization of ETL, we used FIRA with PCBM concentration in chlorobenzene of 0.135 mol/L; the optimum FIRA power of 500 W with a film thickness of 90 nm was achieved. The optimization of the PCBM ETL layer in FPSC showed promising results, which will lead to improved device efficiency and performance. The findings show better charge extraction, reduced charge recombination with a crystallinity value of 66%, charge carrier lifetime of 0.6214 ns, and good transmittance. This contributes to the ongoing efforts to address the challenges associated with the stability and low efficiency of FPSC.

Further efforts should be made to scale up the efficiency of the PCBM ETL layer in FPSC and ensure scalability, which is crucial for the practical application and commercialization of the device. The study introduces a novel approach to FPSCs by optimising the ETL using PCBM combined with FIRA, significantly reducing processing time and enhancing PCE. Key innovations include using lead-free perovskite ($Cs_3Bi_2I_9$), precise

optimisation of PCBM annealing conditions to improve electron extraction, and developing a unique calibration system for thermal processing. These advancements lead to better charge transport, reduced recombination losses, improved device performance, and enhanced scalability and sustainability for FPSCs, making it a significant step toward efficient and eco-friendly solar technologies.

Acknowledgments

This work was performed with the support of the Universiti Kebangsaan Malaysia Research Grant under the Mimos project (RS-2021-003)

Conflict of interest: No conflicts of interest are declared.

References

Aftab, S., Hussain, S., Kabir, F., Aslam, M., Rajpar, A. H., & Al-Sehemi, A. G. (2024). Advances in flexible perovskite solar cells: A comprehensive review. *Nano Energy*, 120. https://doi.org/10.1016/j.nanoen.2023.109112

Bag, A., Radhakrishnan, R., Nekovei, R., & Jeyakumar, R. (2020). Effect of absorber layer, hole transport layer thicknesses, and its doping density on the performance of perovskite solar cells by device simulation. *Solar Energy*, *196*, 177–182. https://doi.org/10.1016/j.solener.2019.12.014

Bai, F., Hu, Y., Hu, Y., Qiu, T., Miao, X., & Zhang, S. (2018). Lead-free, air-stable ultrathin Cs3Bi2I9 perovskite nanosheets for solar cells. *Solar Energy Materials and Solar Cells*, *184*, 15–21. https://doi.org/10.1016/j.solmat.2018.04.032

Bi, Z., Zhang, S., Thandapani, M., Zhu, Y., Zheng, Y., Liem, N. Q., Xiao, X., Xu, G., Guerrero, A., & Xu, X. (2021). High Shunt Resistance SnO2-PbO Electron Transport Layer for Perovskite Solar Cells Used in Low Lighting Applications. *Advanced Sustainable Systems*, *5*(11). https://doi.org/10.1002/adsu.202100120

Bouhjar, F., Derbali, L., & Marí, B. (2020). High performance novel flexible perovskite solar cell based on a low-cost-processed ZnO:Co electron transport layer. *Nano Research*, *13*(9), 2546–2555. https://doi.org/10.1007/s12274-020-2896-4

Cao, K., Zuo, Z., Cui, J., Shen, Y., Moehl, T., Zakeeruddin, S. M., Grätzel, M., & Wang, M. (2015). Efficient screen printed perovskite solar cells based on mesoscopic TiO2/Al2O3/NiO/carbon architecture. *Nano Energy*, *17*, 171–179. https://doi.org/10.1016/j.nanoen.2015.08.009

Cho, A. N., Jang, I. H., Seo, J. Y., & Park, N. G. (2018). Dependence of hysteresis on the perovskite film thickness: Inverse behavior between TiO2 and PCBM in a normal planar structure. *Journal of Materials Chemistry A*, *6*(37), 18206–18215. https://doi.org/10.1039/c8ta04919j

Corzo, D., Tostado-Blázquez, G., & Baran, D. (2020). Flexible Electronics: Status, Challenges and Opportunities. *Frontiers in Electronics*, *1*. https://doi.org/10.3389/felec.2020.594003

Deng, Y., Peng, E., Shao, Y., Xiao, Z., Dong, Q., & Huang, J. (2015). Scalable fabrication of efficient organolead trihalide perovskite solar cells with doctor-bladed active layers. *Energy and Environmental Science*, *8*(5), 1544–1550. https://doi.org/10.1039/c4ee03907f

Erb, T., Zhokhavets, U., Gobsch, G., Raleva, S., Stühn, B., Schilinsky, P., Waldauf, C., & Brabec, C. J. (2005). Correlation between structural and optical properties of composite polymer/fullerene films for organic solar cells. *Advanced Functional Materials*, *15*(7), 1193–1196. https://doi.org/10.1002/adfm.200400521

Eze, M. C., Ugwuanyi, G., Li, M., Eze, H. U., Rodriguez, G. M., Evans, A., Rocha, V. G., Li, Z., & Min, G. (2021). Optimum silver contact sputtering parameters for efficient perovskite solar cell fabrication. *Solar Energy Materials and Solar Cells*, *230*. https://doi.org/10.1016/j.solmat.2021.111185

Fan, L., Ding, Y., Shi, B., Wei, C., Zhang, D., Xie, J., Yu, X., Yan, B., Zhao, Y., & Zhang, X. (2016). Novel insight into the function of PC61BM in efficient planar perovskite solar cells. *Nano Energy*, *27*, 561–568. https://doi.org/10.1016/j.nanoen.2016.08.001

Gao, B., & Meng, J. (2020). High efficiently CsPbBr3 perovskite solar cells fabricated by multi-step spin coating method. *Solar Energy*, *211*, 1223–1229. https://doi.org/10.1016/j.solener.2020.10.045

Gao, Y., Dong, Y., Huang, K., Zhang, C., Liu, B., Wang, S., Shi, J., Xie, H., Huang, H., Xiao, S., He, J., Gao, Y., Hatton, R. A., & Yang, J. (2018). Highly Efficient, Solution-Processed CsPbI2Br Planar Heterojunction Perovskite Solar Cells via Flash Annealing. *ACS Photonics*, *5*(10), 4104–4110. https://doi.org/10.1021/acsphotonics.8b00783

Goje, A. A., Ludin, N. A., Fahsyar, P. N. A., Syafiq, U., Chelvanathan, P., Syakirin, A. D. A. G., Teridi, M. A., Ibrahim, M. A., Su'ait, M. S., Sepeai, S., & Yasir, A. S. H. M. (2024). Review of flexible perovskite solar cells for indoor and outdoor applications. *Materials for Renewable and Sustainable Energy*. https://doi.org/10.1007/s40243-024-00257-8

Goje, A. A., Ludin, N. A., Mat Teridi, M. A., Syafiq, U., Ibrahim, M. A., Nawab, F., & Syakirin, A. A. (2023). Design and Simulation of Lead-free Flexible Perovskite Solar cell Using SCAPS-1D. *IOP Conference Series: Materials Science and Engineering*, *1278*(1), 012004. https://doi.org/10.1088/1757-899x/1278/1/012004

Hamukwaya, S. L., Hao, H., Mashingaidze, M. M., Zhong, T., Tang, S., Dong, J., Xing, J., & Liu, H. (2022). Potassium Iodide-Modified Lead-Free Cs3Bi2I9 Perovskites for Enhanced High-Efficiency Solar Cells. *Nanomaterials*, *12*(21). https://doi.org/10.3390/nano12213751

Hao, M. Y., Wang, H. Y., Wang, Y., Qin, Y., Zhang, J. P., & Ai, X. C. (2020). Effect of energetic distribution of trap states on fill factor in perovskite solar cells. *Journal of Power Sources*, *479*. https://doi.org/10.1016/j.jpowsour.2020.229077

Isah, M., Doroody, C., Rahman, K. S., Rahman, M. N. A., Goje, A. A., Soudagar, M. E. M., Kiong, T. S., Mubarak, N. M., & Zuhdi, A. W. M. (2024). Exploring the impact of defect energy levels in CdTe/Si dual-junction solar cells using wxAMPS. *Scientific Reports*, *14*(1). https://doi.org/10.1038/s41598-024-55616-2

Jackson, K. A. (2004). Kinetic processes : crystal growth, diffusion, and phase transitions in materials. Wiley-VCH Verlag GmbH & Co. KGaA, Weinheim. https://doi.org/10.1002/3527603891

Jiang, H., Jiang, G., Xing, W., Xiong, W., Zhang, X., Wang, B., Zhang, H., & Zheng, Y. (2018). High Current Density and Low Hysteresis Effect of Planar Perovskite Solar Cells via PCBM-doping and Interfacial Improvement. *ACS Applied Materials and Interfaces*, *10*(35), 29954–29964. https://doi.org/10.1021/acsami.8b06020

Karagiannidis, P. G., Kassavetis, S., Pitsalidis, C., & Logothetidis, S. (2011). Thermal annealing effect on the nanomechanical properties and structure of P3HT:PCBM thin films. *Thin Solid Films*, *519*(12), 4105–4109. https://doi.org/10.1016/j.tsf.2011.01.196

Khadka, D. B., Shirai, Y., Yanagida, M., & Miyano, K. (2019). Tailoring the film morphology and interface band offset of caesium bismuth iodide-based Pb-free perovskite solar cells. *Journal of Materials Chemistry C*, *7*(27), 8335–8343. https://doi.org/10.1039/c9tc02181g

Kong, H., Sun, W., & Zhou, H. (2021). Progress in flexible perovskite solar cells with improved efficiency. *Journal of Semiconductors*, 42(10). https://doi.org/10.1088/1674-4926/42/10/101605

Krebs, F. C. (2009). Fabrication and processing of polymer solar cells: A review of printing and coating techniques. In *Solar Energy Materials and Solar Cells*, 93(4), 394–412). https://doi.org/10.1016/j.solmat.2008.10.004

Li, X., Shi, Z., Behrouznejad, F., Hatamvand, M., Zhang, X., Wang, Y., Liu, F., Wang, H., Liu, K., Dong, H., Mudasar, F., Wang, J., Yu, A., & Zhan, Y. (2022). Highly efficient flexible perovskite solar cells with vacuum-assisted low-temperature annealed SnO2 electron transport layer. *Journal of Energy Chemistry*, *67*, 1–7. https://doi.org/10.1016/j.jechem.2021.09.021

Ling, P. S. V., Hagfeldt, A., & Sanchez, S. (2021). Flash infrared annealing for perovskite solar cell processing. *Journal of Visualized Experiments*, *2021*(168), 1–20. https://doi.org/10.3791/61730

Lu, G., He, F., Pang, S., Yang, H., Chen, D., Chang, J., Lin, Z., Zhang, J., & Zhang, C. (2017). A PCBM-Modified TiO2 Blocking Layer

towards Efficient Perovskite Solar Cells. *International Journal of Photoenergy*, *2017*. https://doi.org/10.1155/2017/2562968

Maggioni, G. M., & Mazzotti, M. (2019). A Stochastic Population Balance Equation Model for Nucleation and Growth of Crystals with Multiple Polymorphs. *Crystal Growth and Design*, *19*(8), 4698–4709. https://doi.org/10.1021/acs.cgd.9b00577

Mali, S. S., Patil, J. V., Kim, H., & Hong, C. K. (2018). Synthesis of SnO2 nanofibers and nanobelts electron transporting layer for efficient perovskite solar cells. *Nanoscale*, *10*(17), 8275–8284. https://doi.org/10.1039/c8nr00695d

Malison, P., Bhoomanee, C., Choopun, S., Wongratanaphisan, D., Sagawa, T., & Ruankham, P. (2019). Effects of Sn Incorporation in ZnO Thin Films on Properties of Perovskite Solar Cells. *IOP Conference Series: Materials Science and Engineering*, *526*(1). https://doi.org/10.1088/1757-899X/526/1/012018

Miller, S., Fanchini, G., Lin, Y. Y., Li, C., Chen, C. W., Su, W. F., & Chhowalla, M. (2008). Investigation of nanoscale morphological changes in organic photovoltaics during solvent vapor annealing. *Journal of Materials Chemistry*, *18*(3), 306–312. https://doi.org/10.1039/b713926h

Mohamad Noh, M. F., Teh, C. H., Daik, R., Lim, E. L., Yap, C. C., Ibrahim, M. A., Ahmad Ludin, N., Mohd Yusoff, A. R. Bin, Jang, J., & Mat Teridi, M. A. (2018a). The architecture of the electron transport layer for a perovskite solar cell. *Journal of Materials Chemistry C* 6(4), 682–712. https://doi.org/10.1039/c7tc04649a

Namkoong, G., Mamun, A. A., & Tasnim Ava, T. (2018). Impact of PCBM/C60 electron transfer layer on charge transports on ordered and disroderd perovskite phases and hysteresis-free perovkstie solar cells. *Organic electron,* 56,163-169. https://doi.org/10.1016/j.orgel.2018.02.010

Noh, Y. W., Jin, I. S., Kim, K. S., Park, S. H., & Jung, J. W. (2020). Reduced energy loss in SnO2/ZnO bilayer electron transport layer-based perovskite solar cells for achieving high efficiencies in outdoor/indoor environments. *Journal of Materials Chemistry A*, *8*(33), 17163–17173. https://doi.org/10.1039/d0ta04721j

Ouyang, Z., Yang, M., Whitaker, J. B., Li, D., & Van Hest, M. F. A. M. (2020). Toward Scalable Perovskite Solar Modules Using Blade Coating and Rapid Thermal Processing. *ACS Applied Energy Materials*, *3*(4), 3714–3720. https://doi.org/10.1021/acsaem.0c00180

Ramli, N. F., Fahsyar, P. N. A., Ludin, N. A., Teridi, M. A. M., Ibrahim, M. A., Zaidi, S. H., & Sepeai, S. (2019). Compatibility between compact and mesoporous TiO2 layers on the optimization of photocurrent density in photoelectrochemical cells. *Surfaces and Interfaces*, *17*. https://doi.org/10.1016/j.surfin.2019.100341

Sánchez, S., Hua, X., Günzler, A., Bermúdez-Ureña, E., Septiadi, D., Saliba, M., & Steiner, U. (2020). Flash Infrared Pulse Time Control of Perovskite Crystal Nucleation and Growth from Solution. *Crystal Growth and Design*, *20*(2), 670–679. https://doi.org/10.1021/acs.cgd.9b01083

Sánchez, S., Jerónimo-Rendon, J., Saliba, M., & Hagfeldt, A. (2020a). Highly efficient and rapid manufactured perovskite solar cells via Flash InfraRed Annealing. *Materials Today*, *35*, 9–15. https://doi.org/10.1016/j.mattod.2019.11.003

Sánchez, S., Vallés-Pelarda, M., Alberola-Borràs, J. A., Vidal, R., Jerónimo-Rendón, J. J., Saliba, M., Boix, P. P., & Mora-Seró, I. (2019). Flash infrared annealing as a cost-effective and low environmental impact processing method for planar perovskite solar cells. *Materials Today*, *31*, 39–46. https://doi.org/10.1016/j.mattod.2019.04.021

Shah, S. K., Khan, J., Ullah, I., & Khan, Y. (2017). Optimization of active-layer thickness, top electrode and annealing temperature for polymeric solar cells. *AIMS Materials Science*, *4*(3), 789–799. https://doi.org/10.3934/matersci.2017.3.789

Shahiduzzaman, M., Hossain, M. I., Visal, S., Kaneko, T., Qarony, W., Umezu, S., Tomita, K., Iwamori, S., Knipp, D., Tsang, Y. H., Akhtaruzzaman, M., Nunzi, J. M., Taima, T., & Isomura, M. (2021). Spray Pyrolyzed TiO2 Embedded Multi-Layer Front Contact Design for High-Efficiency Perovskite Solar Cells. *Nano-Micro Letters*, *13*(1). https://doi.org/10.1007/s40820-020-00559-2

Taheri, B., De Rossi, F., Lucarelli, G., Castriotta, L. A., Di Carlo, A., Brown, T. M., & Brunetti, F. (2021). Laser-Scribing Optimization for Sprayed SnO2-Based Perovskite Solar Modules on Flexible Plastic Substrates. *ACS Applied Energy Materials*, *4*(5), 4507–4518. https://doi.org/10.1021/acsaem.1c00140

Tzounis, L., Stergiopoulos, T., Zachariadis, A., Gravalidis, C., Laskarakis, A., & Logothetidis, S. (2017). Perovskite solar cells from small scale spin coating process towards roll-to-roll printing: Optical and Morphological studies. *Materials Today: Proceedings*, *4*(4), 5082–5089. https://doi.org/10.1016/j.matpr.2017.04.117

Vijaya, S., Subbiah, J., Jones, D. J., & Anandan, S. (2023). LARP-assisted synthesis of CsBi 3 I 10 perovskite for efficient lead-free solar cells . *RSC Advances*, *13*(15), 9978–9982. https://doi.org/10.1039/d3ra00365e

Wang, B., Yang, J., Lu, L., Xiao, W., Wu, H., Xiong, S., Tang, J., Duan, C., & Bao, Q. (2020). Interface Engineering of Air-Stable n-Doping Fullerene-Modified TiO2 Electron Transport Layer for Highly Efficient and Stable Perovskite Solar Cells. *Advanced Materials Interfaces*, *7*(6). https://doi.org/10.1002/admi.201901964

Wang, H., Wang, X., Zhang, H., Ma, W., Wang, L., & Zong, X. (2020). Organic−inorganic hybrid perovskites: Game-changing candidates for solar fuel production. *Nano Energy*, 71. https://doi.org/10.1016/j.nanoen.2020.104647

Wang, K. L., Zhou, Y. H., Lou, Y. H., & Wang, Z. K. (2021). Perovskite indoor photovoltaics: opportunity and challenges. In *Chemical Science*,12(36), 11936–11954.. https://doi.org/10.1039/d1sc03251h

Wang, L., Liu, G., Xi, X., Yang, G., Hu, L., Zhu, B., He, Y., Liu, Y., Qian, H., Zhang, S., & Zai, H. (2022). Annealing Engineering in the Growth of Perovskite Grains. *Crystals*, 12(7). https://doi.org/10.3390/cryst12070894

Wang, X., Liman, C. D., Treat, N. D., Chabinyc, M. L., & Cahill, D. G. (2013). Ultralow thermal conductivity of fullerene derivatives. *Physical Review B - Condensed Matter and Materials Physics*, *88*(7). https://doi.org/10.1103/PhysRevB.88.075310

Waykar, R., Bhorde, A., Nair, S., Pandharkar, S., Gabhale, B., Aher, R., Rondiya, S., Waghmare, A., Doiphode, V., Punde, A., Vairale, P., Prasad, M., & Jadkar, S. (2020). Environmentally stable lead-free cesium bismuth iodide (Cs3Bi2I9) perovskite: Synthesis to solar cell application. *Journal of Physics and Chemistry of Solids*, *146*. https://doi.org/10.1016/j.jpcs.2020.109608

Yang, D., Zhang, X., Wang, K., Wu, C., Yang, R., Hou, Y., Jiang, Y., Liu, S., & Priya, S. (2019). Stable Efficiency Exceeding 20.6% for Inverted Perovskite Solar Cells through Polymer-Optimized PCBM Electron-Transport Layers. *Nano Letters*, *19*(5), 3313–3320. https://doi.org/10.1021/acs.nanolett.9b00936

Yang, Z., Chen, W., Mei, A., Li, Q., & Liu, Y. (2021). Flexible MAPbI3 perovskite solar cells with the high efficiency of 16.11% by low-temperature synthesis of compact anatase TiO2 film. *Journal of Alloys and Compounds*, *854*. https://doi.org/10.1016/j.jallcom.2020.155488

Ye, X., Ling, H., Zhang, R., Wen, Z., Hu, S., Akasaka, T., Xia, J., & Lu, X. (2020). Low-temperature solution-combustion-processed Zn-Doped Nb2O5 as an electron transport layer for efficient and stable perovskite solar cells. *Journal of Power Sources*, *448*. https://doi.org/10.1016/j.jpowsour.2019.227419

Yu, B. Bin, Liao, M., Yang, J., Chen, W., Zhu, Y., Zhang, X., Duan, T., Yao, W., Wei, S. H., & He, Z. (2019). Alloy-induced phase transition and enhanced photovoltaic performance: The case of Cs3Bi2I9-xBrx perovskite solar cells. *Journal of Materials Chemistry A*, *7*(15), 8818–8825. https://doi.org/10.1039/c9ta01978b

Zhang, F., Castaneda, J. F., Chen, S., Wu, W., DiNezza, M. J., Lassise, M., Nie, W., Mohite, A., Liu, Y., Liu, S., Friedman, D., Liu, H., Chen, Q., Zhang, Y. H., Huang, J., & Zhang, Y. (2020). Comparative studies of optoelectrical properties of prominent PV materials: Halide perovskite, CdTe, and GaAs. *Materials Today*, *36*, 18–29. https://doi.org/10.1016/j.mattod.2020.01.001

Zhang, S., Wang, Z., Guo, B., & Xu, J. (2021). Secondary nucleation in polymer crystallization: A kinetic view. *Polymer Crystallization*, *4*(3). https://doi.org/10.1002/pcr2.10173

Zhang, W., Lin, Z., Cai, Q. Xu, X., Dong, H., Mu, C. and Zhang, J.-P. (2022). Electron Transport Assisted by Transparent Conductive Oxide Elements in Perovskite Solar Cells. *ChemSusChem*, *4*(4), 112–143. https://doi.org/10.1002/cssc.202102002

Zhong, Y., Hufnagel, M., Thelakkat, M., Li, C., & Huettner, S. (2020a). Role of PCBM in the Suppression of Hysteresis in Perovskite Solar Cells. *Advanced Functional Materials*, *30*(23). https://doi.org/10.1002/adfm.201908920